Applied Radiation and Isotopes 83 (2014) 68–76

Contents lists available at ScienceDirect

Applied Radiation and Isotopes

journal homepage: www.elsevier.com/locate/apradiso

Electron scattering cross sections from anthracene over a broad energy range (0.00001–10,000 eV)

A.G. Sanz [a,*], M.C. Fuss [a], F. Blanco [b], F. Carelli [c], F. Sebastianelli [c], F.A. Gianturco [c], G. García [a,d]

[a] Instituto de Física Fundamental, Consejo Superior de Investigaciones Científicas, Serrano 113-bis, 28006 Madrid, Spain
[b] Departamento de Física Atómica, Molecular y Nuclear, Universidad Complutense de Madrid, Ciudad Universitaria, 28040 Madrid, Spain
[c] Department of Chemistry, "Sapienza" University of Rome, P.le A. Moro 5, 00185 Rome, Italy
[d] Centre for Medical Radiation Physics, University of Wollongong, Wollongong, NSW 2522, Australia

HIGHLIGHTS

- Integral and differential electron cross sections were calculated for anthracene.
- At intermediate energies, ePOLYSCAT and IAM–SCAR methods are smoothly joined.
- A complete set of integral ECS, ICS and TCS from 0.00001 to 10,000 eV is given.
- Computed elastic angular distributions are satisfactorily compared with experiments.

ARTICLE INFO

Available online 3 January 2013

Keywords:
Anthracene
Electron scattering
Elastic cross sections
Inelastic cross sections

ABSTRACT

We report a computational investigation of electron scattering by anthracene ($C_{14}H_{10}$) in the gas phase. Integral and differential cross sections have been calculated by employing two distinct *ab-initio* quantum scattering methods: the symmetry adapted–single centre expansion method (ePOLYSCAT) and a screening corrected form of the independent atom model (IAM–SCAR) at low and high energies, respectively. After a detailed evaluation of the current results, we present a complete set of integral scattering cross sections from 0.00001 to 10,000 eV.

1. Introduction

For the study and the understanding of radiation-induced damage on biological systems, Monte Carlo track structure simulations constitute a very useful tool (Agostinelli et al., 2003; Baró et al., 1995). They allow, in fact, to determine with realistic spatial and temporal resolutions the different scattering processes involved and the distribution of energy deposition along the particle paths. When the primary energetic particles (photons, electrons, ions etc.) pass through biological matter it is already accepted that large quantities of low-energy electrons (LEEs) are produced ($\sim 4 \times 10^4$ by a 1 MeV particle) (Henry, 1979; Pimblott and LaVerne, 2007) and therefore the interaction of these LEEs with biomolecules has been extensively studied during the last decade since they are known to cause severe structural and chemical alterations (Boudaïffa et al., 2000; Cai et al., 2005) at the molecular level. It is therefore mandatory that accurate energy deposition models should also take into account the effects originated by these low-energy electrons, as is indeed the case with the low-energy particle track simulation code (LEPTS) (Roldán et al., 2004; Muñoz et al., 2005). Since these simulations require the cross sections for all involved processes as input data, complete sets of recommended electron scattering cross sections are needed over a wide energy range that could be extended from high energies down to the very low energies of thermalized electrons.

Although these cross sections have been widely studied for different atomic and molecular targets (Trajmar et al.,1983; Brunger and Buckman, 2002; Gulley et al., 1998), due to the difficulties involved in their reliable measurement or calculation, most works have been restricted to the low-energy domain and therefore studies covering the entire energy range are only available for a few biomolecules (Fuss et al., 2010; Muñoz et al., 2007; Manero et al., 2002). To carry out calculations within the high-energy regime, a complete theoretical *ab-initio* treatment is not affordable since all discrete and continuum channels are open and consequently different approximations have to be implemented to make computations manageable. In previous work we have

* Corresponding author. Tel.: +34 91 5616800x943214.
E-mail addresses: ana@iff.csic.es (A.G. Sanz), g.garcia@iff.csic.es (G. García).

0969-8043/$ - see front matter © 2013 Elsevier Ltd. All rights reserved.
http://dx.doi.org/10.1016/j.apradiso.2012.12.015

shown that optical potential calculations assuming that a modified independent-atom description of the molecular targets constitutes a simple and powerful tool at intermediate and high energies (30–5000 eV) (Blanco and García, 2003b, 2004) giving reliable results from diatomic molecules to complex biomolecules (Muñoz et al., 2007; Kato et al., 2012; Maljković et al., 2012; Blanco and García, 2007). Below 100 eV, the symmetry adapted–single centre expansion method developed by Gianturco et al. (1994), Natalense and Lucchese (1999) gives a good representation of the elastic scattering for a wide variety of biomolecules (Gianturco and Lucchese, 2001; Carelli and Gianturco, 2011a; Carelli et al., 2008, 2011b). On the other hand, computational analysis of electron scattering with polyatomic molecules is still fairly limited to few-atoms and few-electrons molecular structures. It is therefore important, from the point of view of testing quantum scattering models, to analyze electron collisions for increasingly more complicated molecules and be able to generate integral and differential cross sections for a wide energy range.

Anthracene is a polycyclic aromatic hydrocarbon (PAH) formed by three linearly condensed rings and is of chief interest in various fields of study. It is broadly used as a scintillator for radiation detectors of high-energy photons, electrons and alpha particles. $C_{14}H_{10}$ is a widespread atmospheric and soil contaminant (Keith and Telliard, 1979; Hamdi et al., 2006) produced by, *e.g.*, fuel combustion, and is therefore, of great environmental and health concern due to its potential toxicity, mutagenicity and carcinogenicity (Stein et al., 1992; Palanikumar et al., 2012). Anthracene molecules, together with other PAHs, are believed to be a major component of the interstellar medium (ISM) given that it is taken to be responsible for the infrared emission features that dominate the spectra of many galactic and extragalactic sources (Vijh et al., 2004). Additionally, being a fairly large molecule, anthracene could serve us as a model system for testing our quantum scattering methods on multi-electron targets.

Electron collisions with anthracene have been studied by several authors. Regarding the excited states of anthracene, von Jager (1969) reported the first electron-impact, energy-loss spectra of condensed-phase anthracene with high-energy electrons (35 keV). Further electron energy-loss measurements for gaseous anthracene at 30 keV impact energy were carried out by Koch et al. (1971), covering an energy-loss range up to 25 eV. Their spectra show a strong feature at around 5 eV and broad unresolved features at higher energy values. Allan (1989) obtained more detailed information of the energy-loss features using a trochoidal electron spectrometer in the low impact energy domain; he also provided the energy-dependence curves corresponding to 0.40, 3.24, 3.59 and 5.23 energy losses and identified the location of the triplet levels in this system. More recently Man et al. (1992) discussed the energy-loss spectra for electron impact energies ranging between 12 and 100 eV and scattering angles from 5 to 40, measured with a conventional perpendicular-crossed beam–beam scattering technique. Further measurements on electron attachment were initially provided by Christophorou et al. (1971), who derived cross sections for electron attachment resonances by means of an electron swarm experiment, showing a sharp peak at thermal energies. Burrow et al. (1987) utilized electron transmission spectroscopy to determine the vertical electron affinities and to characterize the short-lived temporary anion states of gaseous anthracene. Formation of long-lived parent negative ions and fragments from anthracene and other PAHs anions following low-energy electron impact was studied by Tobita et al. (1992), who observed a maximum in the parent negative ion yield curve at energies close to 0.0 eV. Canosa et al. (1994) confirmed the sharp peak close to 0.0 eV and found the rate coefficient of electron attachment to anthracene to be 10^{-9} cm^3 s^{-1}. Regarding integral elastic or total cross sections, neither theoretical nor experimental data appear, to our knowledge, to be available in the literature. Differential cross sections have been only measured by Boechat-Roberty et al. (1997) who provided absolute elastic and inelastic differential cross sections for the anthracene molecule at an incident electron energy of 1 keV.

The aim of this work is therefore to present computed cross sections (CS) for electron scattering with anthracene, obtained by joining together the aforementioned *ab-initio* quantum scattering models: the symmetry adapted–single centre expansion approach (ePOLYSCAT) and the corrected form of the independent-atom model (IAM) called screening-corrected additivity rule (IAM–SCAR), which have been found in previous work to be separately reliable at low and at high energies, respectively. Hence, we provide for the first time a complete set of recommended integral elastic CS, inelastic CS and total scattering cross sections (TCS) in the energy range between 0.00001 and 10,000 eV. We further compute the elastic angular distributions (EDCS) at selected energies over the same energy range examined above and compare their behaviour with the existing experimental data from Boechat-Roberty et al. (1997).

In the following section, we briefly provide the details of both our theoretical methods, while in Section 3 we report our results for the integral cross sections and the angular distributions of the elastic scattering processes at various collision energies. In Section 4 we summarize our work before drawing our conclusions from this study.

2. Theoretical methods: An outline

2.1. Symmetry adapted–single centre expansion (SA–SCE) method

The molecular quantum dynamical method we use to model the low-energy electron interaction with polyatomic molecules has been described previously (Baccarelli et al., 2008; Gianturco and Lucchese, 2004); therefore, we only present here a brief summary.

This approach describes the overall electron–molecule scattering in the time-independent framework within the Born–Oppenheimer approximation. The total wave function of the continuum electron scattered from an N-electron molecular target ($N+1$ e$^-$) is expressed as an antisymmetrized product of one-electron orbitals. The target electronic wave function is given by a single-determinant of Hartree–Fock (HF) orbitals of the neutral ground state target, where the N molecular electrons are considered as keeping their ground state configuration during the scattering process. We further assume the fixed-nuclei (FN) approximation (Huo and Gianturco, 1995), which neglects involving the nuclear motion. Thus, our present treatment shall be limited to the elastic channels and will include rotational excitation effects *via* an adiabatic summing model (Gianturco et al., 1994). Our implementation of the scattering equations is based on expanding any arbitrary three-dimensional function describing a given electron, either a bound or the scattered electron, around a single-centre (SCE), namely the centre of mass of the target:

$$F^{p\mu}(r,\theta,\phi|\boldsymbol{R}) = \frac{1}{r}\sum_m f_{hl}^{p\mu}(r|\boldsymbol{R}) X_{hl}^{p\mu}(\theta,\phi), \quad (1)$$

where μ is a component of the pth irreducible representation of the point group of the molecule (D_{2h} for anthracene) and the h index labels a specific basis function, for a given partial wave l. The angular functions $X_{hl}^{p\mu}(\theta,\phi)$ are symmetry adapted functions

given by the proper combination of spherical harmonics $Y_{lm}(\theta,\phi)$:

$$X_{hl}^{p\mu}(\theta,\phi)=\sum_{m} b_{lmh}^{p\mu} Y_{lm}(\theta,\phi). \quad (2)$$

The coefficients can be obtained from the character tables of the relevant molecular point group (Altman and Herzig, 1994). The resulting quantum scattering equations provide us with a way of evaluating the unknown radial coefficients $f_{hl}^{p\mu}$ for the $(N+1)$th continuum electron scattered off the N-electron target, which takes the following form:

$$\left[\frac{d^2}{dr^2}-\frac{l(l+1)}{r^2}+2(E-\epsilon_\alpha)\right] f_{lh}^{p\mu\alpha}(r|\boldsymbol{R}) = 2\sum_{l'h'p'\mu'\alpha'}\int dr' V_{lh,l'h'}^{p\mu\alpha,p'\mu'\alpha'}(r,r'|\boldsymbol{R}) f_{l'h'}^{p'\mu'\alpha'}(r'|\boldsymbol{R}), \quad (3)$$

where E is the collision energy $E=k^2/2$ and ϵ_α is the electronic eigenvalue for the αth asymptotic state. The (p, μ, α) indices in Eq. (3) now label the symmetry and the corresponding target state of the continuum wave function, and refer to the kernel of the integral operator $\hat{V}$, a sum of diagonal and non-diagonal terms that in principle fully describe the electron–molecule interaction during the collision. As previously anticipated, we assume that the target molecule is initially described by a single state α (the electronic ground state), obtaining the static-exchange (SE) representation of the electron–molecule interaction for the molecular ground-state geometry $\boldsymbol{R}$. Introducing the further assumption of having a local form of exchange interaction, we get a simplified form of the coupled equations

$$\left[\frac{d^2}{dr^2}-\frac{l(l+1)}{r^2}+2(E-\epsilon)\right] f_{lh}^{p\mu}(r|\boldsymbol{R}) = 2\sum_{l'h'} V_{lh,l'h'}^{p\mu}(r|\boldsymbol{R}) f_{l'h'}^{p\mu}(r|\boldsymbol{R}) \quad (4)$$

where the potential coupling elements are given by

$$V_{lh,\,l'h'}^{p\mu}(r|\boldsymbol{R}) = \langle X_{hl}^{p\mu}(\hat{r})|V(\boldsymbol{r}|\boldsymbol{R})|X_{h'l'}^{p\mu}(\hat{r})\rangle = \int d\hat{r} X_{hl}^{p\mu}(\hat{r}) V(\boldsymbol{r}|\boldsymbol{R}) X_{h'l'}^{p\mu}(\hat{r}). \quad (5)$$

The exchange contributions to the potential operator of Eq. (4) are modelled with an energy-dependent local potential chosen to be the free-electron-gas-exchange (FEGE) potential proposed by Hara (1967), V_{FEGE}, as discussed many times before (Telega and Gianturco, 2005; Gianturco and Lucchese, 1998). We further include the dynamical response of the target's bound electrons to the impinging electron, *i.e.*, the correlation and polarization effects acting at short and at large electron–target distances, respectively. This interaction is modelled through the following local energy-independent potential:

$$V_{CP}(\boldsymbol{r}) = \begin{cases} V_{\mathrm{corr}}(\boldsymbol{r}), & \boldsymbol{r} \le r_{\mathrm{match}} \\ V_{\mathrm{pol}}(\boldsymbol{r}), & \boldsymbol{r} > r_{\mathrm{match.}} \end{cases} \quad (6)$$

The V_{CP} model potential contains a short-range correlation contribution V_{corr} which is smoothly connected to the long-range polarization contribution V_{pol}. The short-range term is obtained by defining an average dynamical correlation energy of a single electron within the formalism of the Kohn and Sham variational scheme. The functional derivative of such a quantity with respect to the N-electron density of the molecular target provides a density functional description of the required short-range correlation term. The long-range part of V_{CP} asymptotically depends on the dipole polarizibility of the target in its ground state, given by $-\alpha/2r^4$, which corresponds to including the dipole term in the second-order perturbation expansion of the polarization potential (Lucchese and Gianturco, 1996). This last step provides the so-called static-model-exchange-correlation-polarization (SMECP) approximation for the scattering event in which the potential accounting for the interaction forces between the impinging free electron and the target molecule is now expressed as a sum of three terms, $V_{\mathrm{SMECP}}=V_{ST}+V_{CP}+V_{\mathrm{FEGE}}$, of which V_{ST} describes the static interaction of the scattered electron with the target's nuclei and electrons. Using this model potential, the numerical solutions of the coupled Eq. (4), obtained by means of the standard Green's function technique (Lucchese and Gianturco, 1996), shall produce the relevant K-matrix elements from which the integral and differential elastic cross section will be derived at a specific collision energy (program "ePOLYSCAT": Gianturco et al., 1994; Natalense and Lucchese, 1999).

The above modelling of the full interaction for an impinging electron on a many-electron molecular target has been used by us many times before, usually finding rather good agreement with the available experimental data (Carelli et al., 2008, 2011b; Lucchese and Gianturco, 1996; Telega and Gianturco, 2006).

2.2. Screening-corrected additivity rule (SCAR) method

For the calculation of electron–molecule integral and differential cross sections at intermediate and high energies we apply a corrected form of the independent-atom model (IAM) known as SCAR (screening-corrected additivity rule). All the details for this procedure have been extensively described in previous works (Blanco and García 2002, 2003a, 2003b), where it has been applied to many other molecular species, hence only a brief summary is given here. In the standard IAM treatment, the molecule is approximately substituted by its constituent atoms in their corresponding positions, by assuming that each atom scatters independently and that the molecular binding does not affect the electronic distribution of the atoms. One of the great advantages of this approach is the possibility of obtaining cross sections for a large number of molecular species from the data of a reduced number of atoms. Hence, the first subjects of these calculations are the constituent atoms, namely H and C. Each atomic target is represented by an interacting complex optical potential, $V_{\mathrm{opt}}(\boldsymbol{r})$, whose real part accounts for the elastic scattering of the incident electrons while the imaginary part accounts for the inelastic processes that are considered as "absorption" from the incident beam. This optical potential can be expressed as:

$$V_{\mathrm{opt}}(\mathbf{r}) = V_R(\mathbf{r}) + iV_{\mathrm{abs}}(\mathbf{r}) = V_s(\mathbf{r}) + V_{\mathrm{ex}}(\mathbf{r}) + V_{\mathrm{pol}}(\mathbf{r}) + iV_{\mathrm{abs}}(\mathbf{r}), \quad (7)$$

where the real potential $V_R(\mathbf{r})$ comprises three terms: $V_s(\mathbf{r})$ is the static term derived from the Hartree–Fock calculation of the atomic charge density (Cowan, 1981). The exchange term $V_{\mathrm{ex}}(\mathbf{r})$, which accounts for the indistinguishability between the incident and target electrons, is given by the semiclassical energy-dependent formula derived by Riley and Truhlar (1975). $V_{\mathrm{pol}}(\mathbf{r})$ is the polarization potential which describes the long-range interactions and depends on the target dipole polarizibility, in the form given by Zhang et al. (1992). Finally, the absorption potential $V_{\mathrm{abs}}(\mathbf{r})$, which accounts for the inelastic processes, is based on Staszewska et al. (1983) quasifree model. Initially some divergences were found when results were compared to the available atomic scattering data. After including some improvements such as many-body and relativistic corrections, screening effects inside the atom, local velocity correction and the description of the electrons indistinguishability, the model shows to provide a good approximation for electron–atom scattering (Blanco and García, 2002, 2003a) over a broad energy range. An excellent example of this was obtained for elastic electron–atomic iodine (I) scattering (Zatsarinny et al., 2011), where the optical potential results compared very favourably with those from a more sophisticated Dirac-B-spline R-matrix computation.

For each atom the corresponding radial scattering equation are numerically integrated, and the resulting complex partial wave phase shifts δ_l are used, in combination with the optical theorem,

to generate the atomic scattering amplitudes ($f(\theta)$). Subsequently, the differential ($d\sigma_{el}/d\Omega$), integral elastic (σ_{el}) and the total (σ_{tot}) scattering cross sections are derived as a function of the scattering angle (θ) and the momentum of the incident electrons (k):

$$f(\theta)=\frac{1}{2ik}\sum_{l=0}^{l_{max}}(2l+1)\left(e^{2i\delta_l}+1\right)P_l(\cos\theta),$$

$$\frac{d\sigma_{el}}{d}=|f(\theta)|^2, \tag{8}$$

$$\sigma_{el}=\int\frac{d\sigma_{el}}{d\Omega}\,d\Omega,\qquad \sigma_{tot}=\frac{4\pi}{k^2}Imf(\theta=0). \tag{9}$$

Then, for calculating the cross sections for electron scattering from molecules, one can apply what is commonly known as the additivity rule (AR) (Otvos and Stevenson, 1956; Jiang et al., 1995). In this approach the molecular scattering amplitude $F(\theta)$ is derived from the sum of all the relevant atomic amplitudes $f_i(\theta)$, including the phase coefficients, thus leading to the molecular differential cross sections (DCS) for the target in question as follows:

$$F(\theta)=\sum_{atoms}f_i(\theta)e^{i\mathbf{q}\times\mathbf{r_i}},\quad \frac{d\sigma_{el}^{molecule}}{d\Omega}=\sum_{i,j}f_i(\theta)f_j^*(\theta)\frac{\sin qr_{ij}}{qr_{ij}}, \tag{10}$$

where $\mathbf{q}$ is the momentum transferred in the scattering process, $\mathbf{r_i}$ are the atomic positions and r_{ij} is the distance between the i and j atoms. Integral cross sections (ICS) can then be determined by integrating those DCS, with the sum of the elastic ICS and the absorption ICS (for all inelastic processes except vibrations and rotations) then giving the total cross sections. Alternatively, ICS can be also derived from the atomic ICS in conjunction with the optical theorem (Mott and Massey, 1965),

$$\sigma_{molecule}=\sum_{atoms}\sigma_i \tag{11}$$

Unfortunately, in its original form, we found an inherent contradiction between the ICS derived from these two approaches which suggested that the optical theorem was being violated. This problem, however, was solved by employing a normalization procedure during the computation of the DCS, so that the ICS derived from the two approaches are now entirely consistent (Milosavljević et al., 2008).

At low energies, typically below 100 eV, where atomic cross sections are not small compared to the interatomic distances within the molecule, the IAM approximation fails because the incident electrons are not fast enough to effectively "see" the target molecule as a sum of the individual atoms and multiple scattering within the molecule is therefore no longer negligible. To reduce this limitation we developed the SCAR method (Blanco and García, 2003b, 2004) which accounts for the geometry of the target molecule (atomic positions and bond lengths) by introducing some screening coefficients which modify both differential and integral cross sections, mainly at low energies. The usual additivity rule expressions (Eqs. (10) and (11)) are replaced by modified ones:

$$\sigma^{elast}=\sum_i s_i\sigma_i^{elast},\quad \sigma^{inelast}=\sum_i s_i\sigma_i^{inelast}, \tag{12}$$

$$\frac{d\sigma^{elast}}{d\Omega}\cong(1-X_s)\frac{\sigma^{elast}-\sigma_D}{4\pi}+\left[1+X_S\left(\frac{\sigma^{elast}}{\sigma_D}-1\right)\right]\frac{d\sigma_D}{d\Omega}, \tag{13}$$

where σ_D, $d\sigma_D/d\Omega$, and X_S are defined by:

$$\frac{d\sigma_i^{elast}}{d\Omega}=\sum_i s_i^2\frac{d\sigma_i^{elast}}{d\Omega}+v\sum_{i\neq j}s_is_jf_i(\theta)f_i^*(\theta)\frac{\sin qr_{ij}}{qr_{ij}}, \tag{14}$$

$$\sigma_D=\sum_i s_i^2\sigma_i^{elast}, \tag{15}$$

$$X_S\approx\frac{\int_0^{45^\circ}d\sigma_D/d\Omega\ \sin\theta\ d\theta}{\int_0^{180^\circ}d\sigma_D/d\Omega\ \sin\theta\ d\theta}. \tag{16}$$

where v is the normalization parameter mentioned above. The introduced screening coefficients ($0\le s_i\le 1$) reduce the contribution from each atom to the total cross section. Calculation of s_i coefficients requires data only on the position and the total cross section σ_i of each atom in the molecule (explicit expressions are given in (Blanco and García, 2003b, 2004)).

With this correction the range of validity of the IAM–SCAR method might be extended down to about 30 eV. For intermediate and high energies (30–5000 eV) this method has been proved to be a powerful tool to calculate electron scattering cross sections from a high variety of molecules (Kato et al., 2012; Maljković et al., 2012; Blanco and García, 2007; Do et al., 2012).

3. Results and discussion

In the low-energy range, integral elastic cross sections (ECS) have been computed with the ePOLYSCAT model. The initial target wave function was generated by the Gaussian suite of codes (Frisch et al., 2004) at the Hartree–Fock level and expanded in the 6–311++G (3df, 3pd) basis set. These *ab-initio* calculations yielded for the neutral molecule a total SCF energy of −536.069 Ha and an optimized geometrical configuration in fairly good agreement with experiments (Ketkar et al., 1981). The bound and scattering wave functions were expanded at the centre-of-mass of the target including partial waves up to $l_{max}=60$. The multipolar expansion of the potential VSMECP included terms up to $\lambda_{max}=120$ and the range of integration has been tested for convergence, finally using a radial box size of 15.2 Å. Anthracene belongs to D_{2h} point group and has no dipole moment due to its centro-symmetric geometry. However, it shows a fairly large polarizibility. Using the above basis set, we get a tensorial polarizibility whose components are $\alpha_{xx}=86.72$, $\alpha_{yy}=266.006$ and $\alpha_{zz}=157.514$ u.a., respectively, also in agreement with the experimental data (Tobik and Dal Corso, 2004).

For higher incident electron energies, integral cross sections for anthracene have been computed with the IAM–SCAR model. The corresponding atomic cross sections for C and H were previously calculated and discussed (Blanco and García, 2003a and references therein). Molecular cross sections have been calculated according to the geometrical parameters obtained and used in the previous cross section calculations.

3.1. Integral cross sections

Calculated integral elastic cross sections are shown in Fig. 1. From 0.00001 to 100 eV elastic cross sections were calculated with the ePOLYSCAT scattering theory (solid red line), and in the 1–10,000 eV incident energy range same parameters were computed with the IAM–SCAR model (dashed blue line). We can appreciate in Fig. 1 a significant rise of the elastic cross sections obtained with ePOLYSCAT model at energies above ionization limit which lies around 7.44 eV, while deviating from the IAM–SCAR data at intermediate incident energies, as expected. The exclusion of a model absorption potential at these lower energies usually leads to an overestimation of the integral ECS at incident

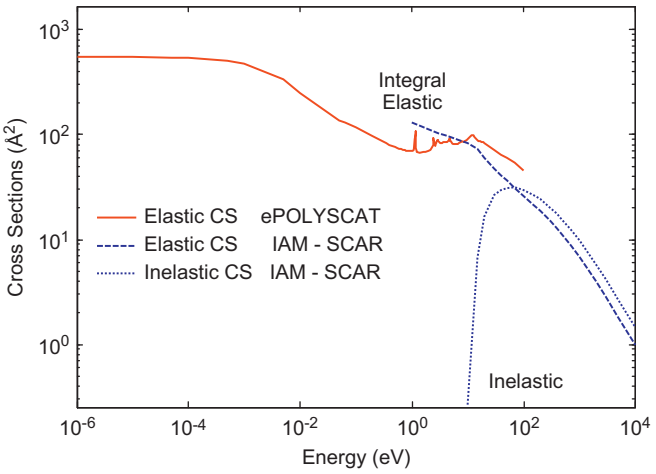

Fig. 1. Theoretical integral cross section for electron scattering by anthracene: (solid red line) ePOLYSCAT elastic cross sections, (dashed blue line) IAM–SCAR elastic cross sections, (dotted blue line) IAM–SCAR inelastic cross sections. (For interpretation of the references to color in this figure legend, the reader is referred to the web version of this article.)

energies above ionization threshold as has been shown by us in earlier works (Blanco and García, 2003a), and afterwards by the Brazilian group (Lee et al., 2007). Indeed, we have recently shown in analogous calculations with hydrogen cyanide (HCN) (Sanz et al., 2012a) that when the absorption term is removed from the SCAR optical potential both methods tend to converge to each other for the higher energies.

In the low-energy domain, we further observe here the presence of various metastable (resonant) anionic states at the electron impact energies of 1.16, 2.46, 2.91, 3.76 and 4.81 eV. They are produced by the temporary capture of the impinging electron by angular momentum trapping from the anthracene molecule (shape resonances). Further analysis of these one-hole (shape) resonances and their evolution into either stabilizing a bound molecular anion or into aromatic fragments by selectively breaking some bonds will be discussed elsewhere (Sanz et al., 2012b). Recommended values for integrated elastic cross section at selected energies from 0.00001 up to 10,000 eV are given in Table 1. According to the previous discussion, from thermalized energies up to ionization potential (7.44 eV), the elastic cross section data are reliably provided by the ePOLYSCAT model within an average uncertainty up to about 10% (Gianturco and Lucchese, 1998, 2001), while above the ionization potential elastic cross sections data obtained by the IAM–SCAR model are preferably considered. For higher incident electron energies (50–10,000 eV) the estimated numerical uncertainty is 10%, as have been discussed by us in previous work (Muñoz et al., 2007; Fuss et al., 2010). At intermediate energies, we obtain an estimated error increasing from 5% at $E=10$ eV up to about 25% at 30 eV, evaluated as half-value of the absolute difference between the present models.

Inelastic cross sections (ICS) calculated through the $iV_a(r)$ absorption term of the IAM–SCAR potential in the 10–10,000 eV energy are also plotted in Fig. 1 (dotted blue line) and shown in Table 1. The present method accounts for the electron–electron interaction processes occurring within that energy range, that is, electronic excitations and ionization, with an estimated uncertainty of 10% (Muñoz et al., 2007; Fuss et al., 2010). The first electronic excited state of the anthracene molecule has been placed at around 3.6 eV by several authors (Boechat-Roberty et al., 1997; Man et al., 1992). However, due to limitations of the present independent atom model at the low-energy region, electronic excited states lying below 10 eV

Table 1
Recommended integral elastic, electronically inelastic (electronic excitation and ionization) and total scattering cross sections for electrons collisions with anthracene from 10^{-5} to 10,000 eV.

Energy (eV)	Elastic (Å²)	Electronic inelastic (Å²)	Total (Å²)
0.00001	551.37		551.37
0.0001	540.95		540.95
0.001	472.21		472.21
0.01	251.78		251.78
0.1	116.42		116.42
0.2	96.66		96.66
0.3	86.41		86.41
0.4	80.44		80.44
0.5	76.55		76.55
0.6	73.86		73.86
0.7	71.97		71.97
0.8	70.67		70.67
0.9	69.86		69.86
1	69.63		69.63
1.17	106.8		106.80
2	69.62		69.62
2.46	92.49		92.49
2.91	88.67		88.67
3	88.68		88.68
3.76	84.66		84.66
4	85.67		85.67
4.81	91.88		91.88
5	86.03		86.03
6	80.82		80.82
7	82.43		82.43
8	87.68		87.68
9	84.82		84.82
10	82.88	0.27	83.15
15	72.52	6.78	79.30
20	60.48	16.63	77.11
30	47.32	26.82	74.14
40	40.88	29.96	70.84
50	36.40	31.08	67.48
70	31.08	31.36	62.44
100	26.24	29.68	55.92
150	21.70	26.80	48.50
200	18.82	24.22	43.04
300	15.15	20.33	35.48
400	12.82	17.53	30.35
500	11.17	15.46	26.63
700	8.96	12.54	21.50
1,000	6.92	9.83	16.74
2,000	4.00	5.82	9.83
3,000	2.86	4.17	7.03
5,000	1.84	2.71	4.55
10,000	0.99	1.47	2.47

are ignored. Additionally, it should be noted that processes involving nuclear motion are not being taken into account in this study; hence, vibrational excitations are neglected. Nevertheless, this restriction is not thought to be significant at the energy range we are interested in here since, due to the non-polar nature of this polycyclic molecule, the vibrational excitation cross sections are usually providing a small increase only of the ECS values.

Recommended theoretical total cross sections are plotted in Fig. 2 and the data are numerically shown in Table 1. Below the ionization potential at 7.44 eV, TCS are given by the ePOLYSCAT computational model. This approximation is considered to be fairly accurate since, up to that ionization threshold, elastic collisions constitute the main scattering process. Above this threshold, we rely on the TCS given by the IAM–SCAR model, which comprises the elastic, electronic excitations and ionization processes. Once more, based on previous studies using both methods (Muñoz et al., 2007; Gianturco and Lucchese, 1998, 2001), we can establish a numerical uncertainty of about 10% for the integral TCS provided by each method within its own energy range of applicability. At intermediate incident energies,

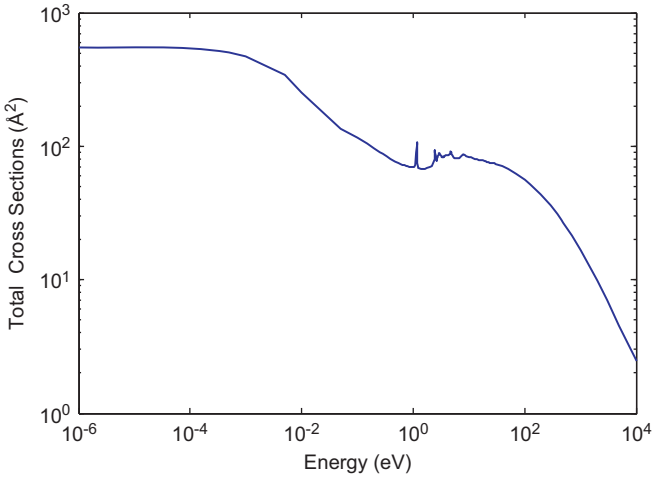

Fig. 2. Recommended theoretical total CS for electron scattering by anthracene.

we determine an estimated uncertainty increasing from 5% at $E=15$ eV up to about 28% at 30 eV, evaluated as half-value from the absolute difference between both models.

Unfortunately, there are no other theoretical computations or experimental data available in the literature with which we can compare the present results. Hence, to estimate the reliability of our calculated values we could consider as a comparison the benzene molecule, since it is formed by a single aromatic ring and accurate experimental data on electron collisions have been recently provided within the energy range we are interested in. Comparison of calculated IAM–SCAR values with experimental data from Cho et al. (2001), Mozejko et al. (1996), Makochekanwa et al. (2003) and Sueoka (1988) indicates a very good behaviour of this theoretical method both for integrated ECS and TCS at intermediate and high incident energies (Blanco and García, 2007). We also find a similar situation in the lower energy regime where ePOLYSCAT elastic cross sections (Gianturco and Lucchese 1998) are in good agreement with the earlier measurements reported by Sueoka (1988), within the error limits of the experiments.

3.2. Elastic differential cross sections

The elastic differential cross sections obtained with the ePOLYSCAT and the IAM–SCAR models over the energy range from 0.00001 to 100 eV and 10 to 10,000 eV, respectively, are presented in Fig. 3 at some selected low, intermediate and large incident energy values. For energies below 1 eV, EDCS derived from ePOLYSCAT model are plotted in Fig. 3a, where we can appreciate that the angular distributions tend to be isotropic as the energy decreases. This behaviour may indicate the presence of a virtual state for anthracene molecule, as will be discussed in detail in a further work (Sanz et al., 2012b). At intermediate energies, the EDCS obtained with ePOLYSCAT (solid red line) and IAM–SCAR (blue dashed line) methods are plotted in Fig. 3b–e: The numerical uncertainty for both theoretical models is estimated to be about 10%, as discussed in the previous section. The angular dependence obtained in the ePOLYSCAT curve is characterized by a shoulder around 40–60° and a broad minimum around 140° at 5 eV which is progressively shifting to lower angles as the impact energy increases (around 80° at 30 eV). The IAM–SCAR angular distribution shows also this broad minimum around 90–110°, which is fairly pronounced around 100 eV but tends to disappear at higher energies. As can be appreciated in these figures, at 15 eV of incident energy both calculations are almost identical, within 4%, for scattering angles between 80° and 160°. For higher impact energies there is still good agreement between both EDCS curves, within 15% from 60° to 180° and 20% from 50° to 180° at 20 and 30 eV, respectively. At lower energies, the agreement worsens, as is to be expected from the low-energy failings of the IAM approximation. One should also note that the EDCSs calculated with the ePOLYSCAT procedure are generally larger at intermediate and large scattering angles. As already pointed out, this is a consequence of omitting absorption effects from model optical potentials within the ePOLYSCAT modelling of the interaction forces, a feature which particularly overestimates DCS values within this angular range (Lee et al., 2007). The EDCSs for higher incident energies as calculated with the IAM–SCAR method are shown in Fig. 3f.

The measurements of Boechat-Roberty et al. (1997) have provided elastic differential cross sections from 0° to 20° and at an incident electron energy of 1 keV. These experimental data have been measured using a crossed-beam configuration which consists of a gas inlet system forming 90° with the electron beam direction produced by an electron gun. Scattered electrons are then evaluated by a Wien-filter electron analyzer and a channeltron detector. The authors stated that the energy and angular resolution of their apparatus is limited to 0.5 eV and 0.23°, respectively, and they therefore estimated the overall uncertainty to be around 8%. We report in Fig. 4 our present computed IAM–SCAR elastic differential cross sections (dashed blue line) together with the experimental data from Boechat-Roberty et al. (green dots). As this figure shows, the results from the IAM–SCAR theory follow very well the experimental data, attaining identical angle dependence. This good performance of the model should be somewhat expected since our optical potential method already showed good angular behaviour at high impact energies for a large variety of molecular targets (Muñoz et al., 2007; Marinković et al., 2008).

According to our knowledge, there are no other experimental or theoretical elastic differential cross sections values available in the literature to compare with our present data. Therefore, as mentioned earlier on in this paper, we have to rely on the good agreement achieved by both ePOLYSCAT and IAM–SCAR models when applied to benzene molecule. In the low-energy regime, Cho et al. (2001) and Gulley and Buckman (1999), compare their experimental EDCS values from 1.1 to 40 eV and at 8 and 20 eV, respectively, with theoretical ePOLYSCAT data, where both sets of experiments show good agreement at angles below 60°. Additionally, in the 20–70 eV region, our IAM–SCAR calculations are in agreement with the EDCS data measured by Kato et al. (2009) for angles above 50°, although some discrepancies were found for smaller angles. For energies above 100 eV these discrepancies disappear, thereby showing excellent agreement with the experiments in the entire angular range. Below 40–50° several authors have shown the presence of a "shoulder" in the angular distribution curve, both from the experimental (Cho et al., 2001; Sanches et al., 2008) and the theoretical side (Bettega et al., 2000). In a very recent work Jones et al. (2012) claimed the existence of a strong resemblance between pyrimidine and benzene molecules electron-scattering angular behaviour at 15 and 30 eV. Maljković et al. (2009) therefore compared their experimental EDCSs for pyrimidine with our theoretical IAM–SCAR data. In accordance with benzene molecule, theory follows experimental data above 50° but fails to reproduce the "shoulder" around 40° at intermediate energies. Differential elastic cross sections for benzene (red asterisks), pyrimidine (green dots) and anthracene (solid blue line) are shown in Fig. 5 for a comparison at 50 eV. Although anthracene cross sections are quantitatively higher by a factor of 3, both EDCS values show similar angular distributions, as better appreciated when scaling our present anthracene calculated data.

From the above discussion we can therefore conclude that for energies below the ionization threshold (7.44 eV) we can safely rely on the data obtained with the ePOLYSCAT model, while at

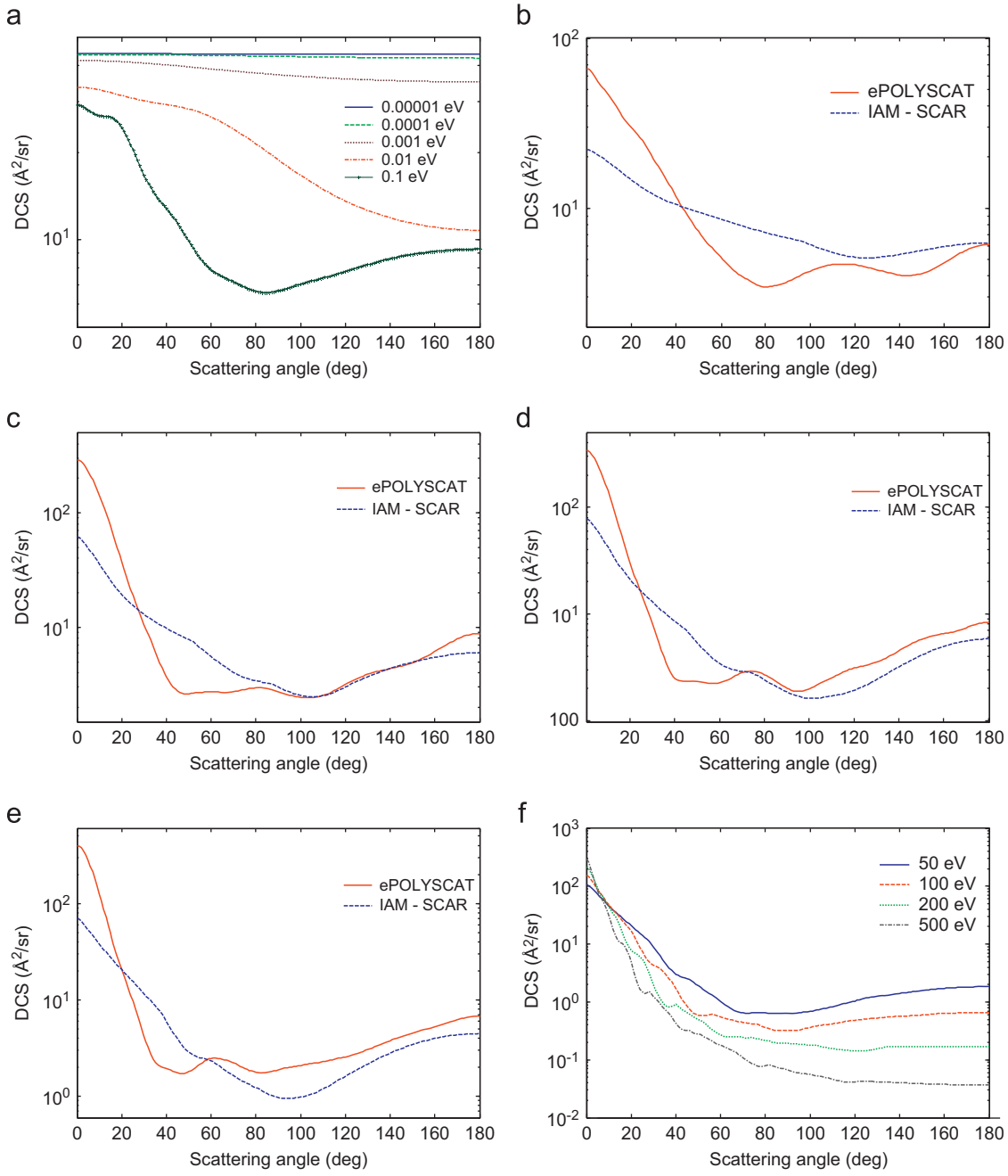

Fig. 3. Angular dependence of differential cross sections for elastic electron scattering from anthracene at different incident energies. Part (a) shows EDCS calculated with ePOLYSCAT model at low incident energies (0.00001–0.1 eV). (b)–(d): (solid red line) ePOLYSCAT elastic differential cross sections, (dashed blue line) IAM–SCAR elastic differential cross sections. Part (f) shows EDCS calculated with IAM–SCAR model at high incident energies (50–500 eV). (For interpretation of the references to color in this figure legend, the reader is referred to the web version of this article.)

intermediate energies (10–70 eV) we expect the ePOLYSCAT theory to give a more realistic picture in the lower angular range below 50°, while the IAM–SCAR procedure provides instead a better agreement for higher angles up to 180°. For energies above 100 eV, the IAM–SCAR theory has been shown in this, and previous, work to give accurate data over the whole angular range of electron distributions.

4. Conclusions

In this study we have reported calculated electron–molecule collisional data that deal with the anthracene molecule. We have shown theoretical cross sections for integral elastic, inelastic and total scattering processes, together with elastic angular distributions from very low energies (0.00001 eV) up to 10,000 eV. Note that we provide here for the first time a complete set of integral cross section data on electron collisions with anthracene, by applying two different *ab-initio* methods: the symmetry adapted–single centre expansion approach (ePOLYSCAT) for energies up to 100 eV and a screening-corrected form of the independent-atom model (IAM–SCAR) for intermediate and high energies. Although there are no equivalent data available for comparison in the literature, by comparing our calculated electron–molecule collisional data on analogous molecules, such as benzene, to measurements published recently (Cho et al., 2001; Makochekanwa et al.,

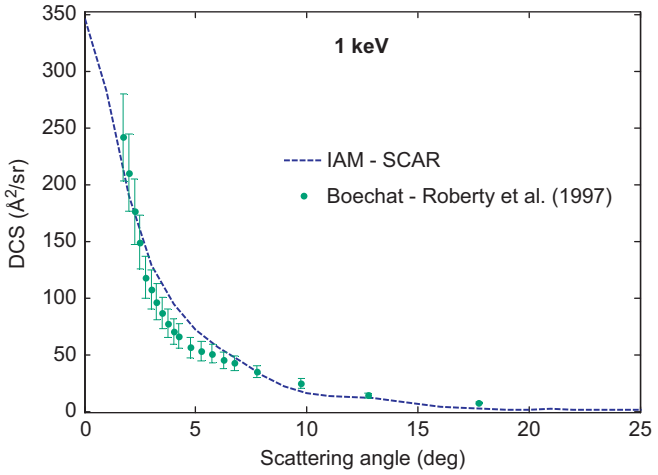

Fig. 4. Comparison of differential elastic cross sections for anthracene with available experimental data at 1 keV: (dashed blue line) present EDCS calculated with IAM–SCAR model, (green dots) measurements from Boechat-Roberty et al. (1997). (For interpretation of the references to color in this figure legend, the reader is referred to the web version of this article.)

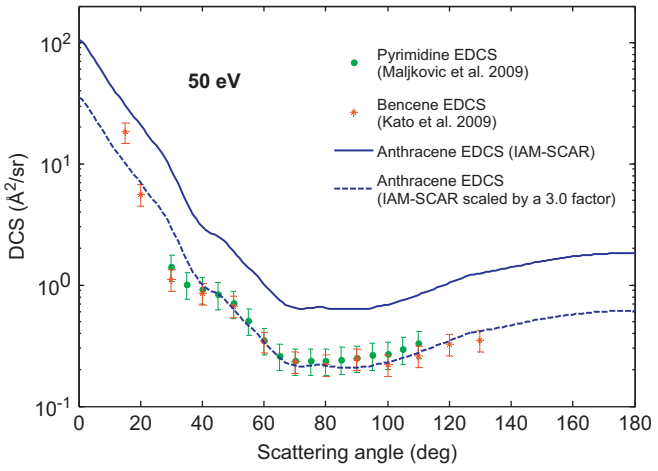

Fig. 5. Angular dependence of differential cross sections for elastic electron scattering from anthracene, benzene and pyrimidine at 50 eV incident energy. (green dots) experimental EDCS for pyrimidine given in Maljković et al. (2009), (red asterisks) experimental data for benzene given in Kato et al. (2009), (solid blue line) present EDCS for anthracene calculated with the IAM–SCAR model, (dashed blue line) anthracene EDCS calculated with the IAM–SCAR model and scaled by a factor of 3. (For interpretation of the references to color in this figure legend, the reader is referred to the web version of this article.)

2003), we can reasonably conclude that both methods are able to yield a reasonable approximation to the experimental quantities, each within its respective energy range of applicability (within 10%) and within 25% at intermediate energies (20–50 eV). Additionally, we provide elastic differential cross sections that are all showing good agreement with the few available experimental data, as those measured by Boechat-Roberty et al. (1997) at an incident electron energy of 1 keV.

We can conclude that by employing a combination of the computational/theoretical methods described in the present study allows one to obtain reliable electron scattering data over a very broad energy range and even for multi-electron systems such as anthracene. These data are thus providing very relevant parameters for radiation-based biomedical applications and in particular they allow us to get benchmark parameters for electron-induced damage in biomolecular systems. Therefore, the present result becomes a promising tool whenever one is aiming to study more complex biological targets in the context of producing computational evidence of the effects on such systems from electron attack. We would like to also point out, however, the persistent need of carrying out further investigations for this scattering system, both from the theoretical and experimental sides, in order to better provide possible sources of comparisons between different approaches.

Acknowledgements

This work is partially supported by the Spanish Ministerio de Economía y Competitividad (Project FIS2009-10245) and the EU/ESF COST Action MP1002 "Nanoscale Insights into Ion Beam Cancer Therapy (Nano-IBCT)". MCF is granted by the Comunidad Autónoma de Madrid local goverment. One of us (FAG) also thanks the Italian MUIR for support through the PRIN 2009-2012 projects.

References

Agostinelli, S., et al., 2003. GEANT4—a simulation tool kit. Nucl. Instrum. Methods Phys. Res., Sect. A 506, 250–303.
Allan, M., 1989. Study of triplet states and short-lived negative ions by means of electron impact spectroscopy. J. Electron Spectrosc. Relat. Phenom. 48, 219–350.
Altman, S.L., Herzig, P., 1994. Point-Group Theory Tables. Oxford University Press, Oxford.
Baccarelli, I., Gianturco, F.A., Grandi, A., Sanna, N., 2008. Metastable anion fragmentations after resonant attachment: deoxyribosic structures from quantum electron dynamics. Int. J. Quantum Chem. 108, 1878–1887.
Baró, J., Sempau, J., Fernández-Varea, J.M., Salvat, F., 1995. PENELOPE: an algorithm for Monte Carlo simulation of the penetration and energy loss of electrons and positrons in matter. Nucl. Instrum.Methods. Phys. Res., Sect. B 100, 31–46.
Bettega, M.H.F., Winstead, C., McKoy, V., 2000. Elastic scattering of low-energy electrons by benzene. J. Chem. Phys. 112, 8806–8812.
Blanco, F., García, G., 2002. Improvements on the imaginary part of a non-empirical model potential for electron scattering (30 to 10000 eV energies). Phys. Lett. A 295, 178–184.
Blanco, F., García, G., 2003a. Improvements on the quasifree absorption model for electron scattering. Phys. Rev. A: At. Mol. Opt. Phys.. 67, 022701.
Blanco, F., García, G., 2003b. Screening corrections for calculation of electron scattering from polyatomic molecules. Phys. Lett. A 317, 458–462.
Blanco, F., García, G., 2004. Screening corrections for calculation of electron scattering differential cross sections from polyatomic molecules. Phys. Lett. A 330, 230–237.
Blanco, F., García, G., 2007. Calculated cross sections for electron elastic and inelastic scattering from DNA and RNA bases. Phys. Lett. A 360, 707–712.
Boechat-Roberty, H.M., Roccoz, M.L.M., Lucas, C.A., Fernandes, M.B., de Souza, G.G.B., 1997. Generalized oscillator strength for the B-1(3u) < −(1)A(g) transition of anthracene, as determined by electron energy-loss spectroscopy. J. Phys. B: At. Mol. Opt. Phys. 30, 3369–3377.
Boudaïffa, B., Cloutier, P., Hunting, D., Huels, M.A., Sanche, L., 2000. Resonant formation of DNA strand breaks by low-energy (3 to 20 eV) electrons. Science 287, 1658–1660.
Brunger, M.J., Buckman, S.J., 2002. Electron–molecule scattering cross-sections. I. Experimental techniques and data for diatomic molecules. Phys. Rep. 357, 215–458.
Burrow, P.D., Michejda, J.A., Jordan, K.D., 1987. Electron transmission study of the temporary negative ion states of selected benzenoid and conjugated aromatic hydrocarbons. J. Chem. Phys. 86, 9–24.
Cai, Z., Cloutier, P., Hunting, D., Sanche, L., 2005. Comparison between X-ray photon and secondary electron damage to DNA in vacuum. J. Phys. Chem. B 109, 4796–4800.
Canosa, A., Parent, D.C., Pasquerault, D., Gomet, J.C., Laubé, S., Rowe, B.R., 1994. Electron attachment to anthracene—a FALP measurement of the rate coefficient at room temperature. Chem. Phys. Lett. 228 (26), 1994.
Carelli, F., Sebastianelli, F., Baccarelli, I., Gianturco, F.A., 2008. Following electron attachment to CS ((1)Sigma): quantum scattering calculations of the lowest resonant state. Int. J. Mass spectrom. 277, 155–161.
Carelli, F., Gianturco, F.A., 2011a. On the relative "transparency" of gas-phase coronene molecules to low-energy electrons: effects on the interstellar medium. Astrophys. J. 743, 151.
Carelli, F., Sebastianelli, F., Satta, M., Gianturco, F.A., 2011b. Gas-phase route to polycyclic aromatic hydrocarbon formation in protoplanetary atmospheres: role of stabilized benzene anions. MNRAS 415, 425–430.
Cho, H., Gulley, R.J., Sunohara, K., Kitajima, M., Uhlmann, L.J., Tanaka, H., Buckman, S.J., 2001. Elastic electron scattering from C_6H_6 and C_6F_6. J. Phys. B: At. Mol. Opt. Phys. 34, 1019–1038.

Christophorou, L.G., McCorkle, D.L., Carter, J.G., 1971. Cross sections for electron attachment resonances peaking at subthermal energies. J. Chem. Phys. 54, 253–260.
Cowan, R.D., 1981. The Theory of Atomic Structure and Spectra. University of California Press, London.
Do, T.P.T., Nixon, K.L., Fuss, M., García, G., Blanco, F., Brunger, M.J., 2012. Electron impact excitation of the (a) over-tilde B-3(1u) electronic state in C_2H_4: an experimentally benchmarked system? J. Chem. Phys. 136, 184313.
Frisch, M.J., Trucks, G.W., Schlegel, H.B., et al., 2004. Gaussian 03. Gaussian Inc., Wallingford, CT, revision c.02.
Fuss, M., Muñoz, A., Oller, J., Blanco, F., Hubin-Franskin, M.J., Almeida, D., Limão - Vieira, P., García, G., 2010. Electron–methane interaction model for the energy range 0.1–10000 eV. Chem. Phys. Lett. 486, 110–115.
Gianturco, F.A., Lucchese, R.R., Sanna, N., 1994. Calculation of low-energy elastic cross-sections for electron-CF4 scattering. J. Chem. Phys. 100, 6464–6471.
Gianturco, F.A., Lucchese, R.R., 1998. One-electron resonances and computed cross sections in electron scattering from the benzene molecule. J. Chem. Phys. 108, 6144–6159.
Gianturco, F.A., Lucchese, R.R., 2001. J. Chem. Phys. Electron scattering from gaseous SF6: comparing calculations with experiments 114, 3429–3439.
Gianturco, F.A., Lucchese, R.R., 2004. Resonant capture of low-energy electrons by gas-phase glycine: a quantum dynamics calculation. J. Phys. Chem. A 108, 7056–7062.
Gulley, R.J., Buckman, S.J., 1999. Absolute elastic electron scattering from benzene. J. Phys. B: At. Mol. Opt. Phys. 32, L405–L409.
Gulley, R.J., Lunt, S.L., Ziesel, J.P., Field, D., 1998. Very low-energy electron scattering from benzene and deuterated benzenes. J. Phys. B: At. Mol. Opt. Phys. 31, 2735–2751.
Hamdi, H., Manusadzianas, L., Aoyama, I., Jedidi, N., 2006. Effects of anthracene, pyrene and benzo[*a*]pyrene spiking and sewage sludge compost amendment on soil ecotoxicity during a bioremediation process. Chemosphere 65, 1153–1162.
Hara, S.J., 1967. Scattering of slow electrons by hydrogen molecules. J. Phys. Soc. Jpn. 22, 710–718.
Henry, W.H., 1979. ICRU Technical Report 31: Average Energy Required to Produce an Ion Pair. International Commission on Radiation Units and Measurements, Washington, DC.
Huo, W.H., Gianturco, F.A., 1995. Computational Methods for Electron–Molecule Collisions. Plenum, New York.
Jiang, Y., Sun, J., Wan, L., 1995. Total cross-sections for electron-scattering by polyatomic-molecules at 10–1000 eV—H_2S, SIH_4, CH_4, CF_4, CCl_4, SF_6, C_2H_4, CCl_3F, $CClF_3$, and CCl_2F_2. Phys. Rev. A: At. Mol. Opt. Phys. 52, 398–403.
Jones, D.B., Bellm, S.M., Limão-Vieira, P., Brunger, M.J., 2012. Low-energy electron scattering from pyrimidine: similarities and differences with benzene. Chem. Phys. Lett. 535, 30–34.
Kato, H., Anzai, K., Ishihara, T., Hoshino, M., Blanco, F., García, G., Limão-Vieira, P., Brunger, M.J., Buckman, S.J., Tanaka, H., 2012. A study of electron interactions with silicon tetrafluoride: elastic scattering and vibrational excitation cross sections. J. Phys. B: At. Mol. Opt. Phys. 45, 095204.
Kato, H., García, M.C., Asahina, T., Hoshino, M., Makochekanwa, C., Tanaka, H., 2009. Absolute elastic differential cross sections for electron scattering by $C_6H_5CH_3$ and $C_6H_5CF_3$ at 1.5–200 eV: a comparative experimental and theoretical study with C_6H_6. Phys. Rev. A 79, 062703.
Keith, L.H., Telliard, W.A., 1979. Priority pollutants I—a perspective view. Environ. Sci. Technol. 13, 416–423.
Ketkar, S.N., Kelley, M., Fink, M., Ivey, R.Ch., 1981. On an electron-diffraction study of the structures of anthraquinone and anthracene. J. Mol. Struct. 77, 127–138.
Koch, E.E., Kunstreich, S., Otto, A., 1971. Measurements of electron energy losses and VUV-reflectivity of anthracene single crystals. Opt. Commun. 2, 365–369.
Lee, M.T., Iga, I., Machado, L.E., Brescansin, L.M., Castro, E.A. y, Sanches, I.P., de Souza, G.L.C., 2007. Improvement on the complex optical potential for electron collisions with atoms and molecules. J. Electron. Spectrosc. Relat. Phenom. 155, 14–20.
Lucchese, R.R., Gianturco, F.A., 1996. One-electron resonances in electron scattering from polyatomic molecules. Int. Rev. Phys. Chem. 15, 429–466.
Makochekanwa, C., Sueoka, O., Kimura, M., 2003. Comparative study of electron and positron scattering from benzene (C_6H_6) and hexafluorobenzene (C_6F_6) molecules. Phys. Rev. A 68, 032707.
Maljković, J.B., Blanco, F., García, G., Marinković, B.P., Milosavljević, A.R., 2012. Absolute cross sections for elastic electron scattering from methylformamide. Phys. Rev. A 85, 042723.
Maljković, J.B., Milosavljević, A.R., Blanco, F., Šević, D., García, D., Marinković, B.P., G., 2009. Absolute differential cross sections for elastic scattering of electrons from pyrimidine. Phys. Rev. A 79, 052706.
Man, K.F., Trajmar, S., McConkey, J.W., Ratliff, J.M., Khakoo, M., 1992. Excitation of anthracene ($C_{14}H_{10}$) by electron impact. J. Phys. B: At. Mol. Opt. Phys. 25, 5245–5256.
Manero, F., Blanco, F., García, G., 2002. Electron scattering cross sections of fluoromethanes in the energy range from 0.1 to 10 keV. Phys. Rev. A 66, 032714.
Marinković, B.P., Blanco, F., Šević, D., Pejčev, V., García, G., Filipović, D.M., Pavlović, D., Mason, N.J., 2008. Elastic scattering of electrons from alanine. Int. J. Mass Spectrom. 277, 300–304.
Milosavljević, A.R., Blanco, F., Maljković, J.B., Šević, D., García, G., Marinković, B.P., 2008. Absolute cross sections for elastic electron scattering from 3-hydroxy-tetrahydrofuran. New J. Phys. 10, 103005.
Mott, N.F., Massey, H.S.W., 1965. The Theory of Atomic Collisions, Third Eds. Oxford University Press, Oxford, UK.
Mozejko, P., Kasperski, G., Szmytkowski, C., Karwasz, G.P., Brusa, R.S., Zecca, A., 1996. Absolute total cross section measurements for electron scattering on benzene molecules. Chem. Phys. Lett. 257, 309–313.
Muñoz, A., Oller, J.C., Blanco, F., Gorfinkiel, J., Limão-Vieira, P., García, G., 2007. Electron-scattering cross sections and stopping powers in H_2O. Phys. Rev. A 76, 052707.
Muñoz, A., Pérez, J.M., García, G., Blanco, F., 2005. An approach to Monte Carlo simulation of low-energy electron and photon interactions in air. Nucl. Instrum. Methods Phys. Res., Sect. A 536, 176–188.
Natalense, A.P.P., Lucchese, R.R., 1999. Cross section and asymmetry parameter calculation for sulfur 1s photoionization of SF6. J. Chem. Phys. 111, 5344–5348.
Otvos, J.W., Stevenson, D.P., 1956. Cross-sections of molecules for ionization by electrons. J. Am. Chem. Soc. 78, 546–551.
Palanikumar, L., Kumaraguru, A.K., Ramakritinan, C.M., Anand, M., 2012. Genotoxic assessment of anthracene and benzo[*a*]pyrene to milkfish *Chanos chanos*. Toxicol. Environ. Chem. 94, 350–363.
Pimblott, S.M., LaVerne, J.A., 2007. Production of low-energy electrons by ionizing radiation. Radiat. Phys. Chem. 76, 1244–1247.
Riley, M.E., Truhlar, D.G., 1975. Approximations for the exchange potential in electron scattering. J. Chem. Phys. 63, 2182–2192.
Roldán, A.M., Pérez, J.M., Blanco, F., Williart, A., García, G., 2004. Energy deposition model of low energy electrons (10–10,000 eV) in air. J. Appl. Phys. 95, 5865–5870.
Sanches, I.P., Sugohara, R.T., Rosani, L., Lee, M.-T., Iga, I., 2008. Cross sections for elastic electron collisions on two hydrocarbon compounds: *n*-butane and benzene in the intermediate-energy range. J. Phys. B: At. Mol. Opt. Phys. 41, 185202.
Sanz, A.G., Carelli, F., Sebastianelli, F., Gianturco, F.A., García, G., 2012b. New J. Phys., unpublished.
Sanz, A.G., Fuss, M.C., Blanco, F., Sebastianelli, F., Gianturco, F.A., García, G., 2012a. Electron scattering cross sections from HCN over a broad energy range (0.1–10000 eV): influence of the permanent dipole moment on the scattering process. J. Chem. Phys. 137, 124103.
Stein, J.E., Collier, T.K., Reichert, W.L., Casillas, E., Hom, T., Varanasi, U., 1992. Bioindicators of contaminant exposure and sublethal effects—studies with benthic fish in puget-sound, Washington. Environ. Toxicol. Chem. 11, 701–714.
Staszewska, G., Schwenke, D.W., Thirumalai, D., Truhlar, D.G., 1983. Quasifree-scattering model for the imaginary part of the optical potential for electron scattering. Phys. Rev. A 28, 2740–2751.
Sueoka, O., 1988. Total cross-section measurements for positron and electron-scattering on benzene molecules. J. Phys. B: At. Mol. Opt. Phys. 21, L631–L635.
Telega, S., Gianturco, F.A., 2005. Vibrational inelastic electron-H_2 scattering revisited: numerically converged coupled channels space frame calculations with model interactions. Eur. Phys. J. D 36, 271–280.
Telega, S., Gianturco, F.A., 2006. Modelling electron-N_2 scattering in the resonant region—integral cross-sections from space fixed coupled channel calculations. Eur. Phys. J. D 38, 495–500.
Tobik, J., Dal Corso, A., 2004. Electric fields with ultrasoft pseudo-potentials: applications to benzene and anthracene. J. Chem. Phys. 120, 9934–9941.
Trajmar, S., Register, D.F., Chutjian, A., 1983. Electron-scattering by molecules. 2. Experimental methods and data. Phys. Rep. 97, 219–356.
Tobita, S., Meinke, M., Illenberger, E., Christophorou, L., Baumgartel, H., Leach, S., 1992. Polycyclic aromatic hydrocarbons: negative ion formation following low energy (0–15 eV) electron impact. Chem. Phys. 161, 501–508.
Vijh, U.P., Witt, A.N., Gordon, K.D., 2004. Discovery of blue luminescence in the red rectangle: possible fluorescence from neutral polycyclic aromatic hydrocarbon molecules? Astrophys. J. 606, L65–L68.
von Jager, J., 1969. Energy losses of monochromatic electrons in condensed aromatic hydrocarbons. Ann. Phys., Lpz 7, 147.
Zatsarinny, O., Bartschat, K., García, G., Blanco, F., Hargreaves, L.R., Jones, D.B., Murrie, R., Brunton, J.R., Brunger, M.J., Hoshino, M., Buckman, S.J., 2011. Electron-collision cross sections for iodine. Phys. Rev. A 83, 042702.
Zhang, X.Z., Sun, J.F., Liu, Y.F., 1992. A new approach to the correlation polarization potential-low-energy electron elastic scattering by He atoms. J. Phys. B: At. Mol. Phys. 25, 1893–1897.